Comparison between two nonlocal criteria: A case study on pressurized holes

Available online at www.sciencedirect.com

ScienceDirect

Procedia Structural Integrity 33 (2021) 456–464

Structural Integrity Procedia

www.elsevier.com/locate/procedia

IGF26 - 26th International Conference on Fracture and Structural Integrity

Comparison between two nonlocal criteria: A case study on pressurized holes

A. Sapora[a], G. Efremidis[b], P. Cornetti[a]*

[a]*Department of Structural Engineering and Geotechnics, Politecnico di Torino, Corso Duca degli Abruzzi 24, 10129 Torino, Italy*
[b]*Department of Civil Engineering, University of Thessaly, Pedion Areos, 38334 Volos, Greece*

Abstract

Two nonlocal approaches are applied to the borehole geometry, i.e. a circular hole in an infinite elastic medium subjected to internal pressure. The former approach lays in the framework of Gradient Elasticity (GE), which results nonlocal in the strict sense, being based on a nonlocal constitutive relationship. Changing the stress field as the geometry (i.e., the radius of the hole) varies, the related stress concentration factor can be thought as the critical failure parameter. The latter approach is the Finite Fracture Mechanics (FFM), well-consolidated in the framework of brittle fracture. Whereas the model belongs to classical linear elasticity, it reveals nonlocal in a loose sense: the failure condition is no more punctual, but achieved when two average requirements on the stress and the energy ahead of the notch tip are simultaneously fulfilled. The two approaches, although different, present some similarities, both involving a characteristic length. It will be shown that the GE and FFM predictions are in excellent agreement when the two lengths are properly defined.

Keywords: pressurized hole; crack initiation; Gradient Elasticity; Finite Fracture Mechanics

1. Introduction

Higher order theories in elasticity have been proposed in order to account for the effect of microstructure (i.e. flaws, cavities, holes, grain interfaces, inclusions, etc.) and to solve various problems for deformation and fracture

* Corresponding author. Tel.: +39-011-090-4901
E-mail address: pietro.cornetti@polito.it

10.1016/j.prostr.2021.10.052

phenomena (see for example Mindlin 1965 and Aifantis 1984, 1987, 1992). On the other hand, classical elasticity cannot describe problems dominated by microstructural effects, since their influence is not properly accounted by the standard continuum models. As for the gradient theory, there is a plethora of gradient-dependent constitutive equations that can be used to interpret size effects, i.e. the dependence of strength and other mechanical properties of the material on the size of the specimen (see for example Efremidis et al. 2001, Aifantis 2003). Moreover, for stress concentration problems, due the pronounced effect of microstructure, they have to be included, into the expression for the strain energy, some additional parameters characterizing the non-locality. This means that the state at a point depends also on the deformation state at neighboring points (Eringen et al. 1972, Eringen 1983, Kunin 1983). The first (or the second, etc.) gradient of the strain field may be considered as such an additional parameter because it characterizes spatial differences in elastic states at neighboring points. By including such non-local terms in the strain energy expression of a deformable elastic body, new modified constitutive equations appear and the relevant gradient theories are developed. Consequently, classical elasticity does not present any intrinsic length scale because it incorporates only the nearest neighbor interaction through the definition of the elastic strain energy density of a deformable body. An intrinsic length scale appears when the forces between particles are extended to include neighbor interactions. Thus, the gradient elasticity may be considered as a higher-order approximation of a fully non-local theory (Aifantis 1992, Askes and Aifantis 2011). The addition of higher order gradients in the governing equations takes into account: a) the non-locality of the physical state of the system in an approximate way, and b) the physical nature of the interactions between the smallest structural particles of the material. Concerning the gradient coefficients, which introduced phenomenologically, in conjunction with the gradient terms, it can be said that they characterize the influence (or the importance) of these terms into the solution of the problem (Aifantis 2003, 2020).

Different criteria based on a critical distance have been proposed to assess the brittle failure behaviour of notched components over the last three decades (Taylor 2007), allowing to overcome the drawbacks rising from Linear Elastic Fracture Mechanics (LEFM). The basic assumption of these approaches is that failure takes place when either the punctual or averaged stress or an energy-related quantity at a finite distance from the notch tip reaches a critical value. Such a distance results a material constant, being proportional to $l_{ch} = (K_{Ic} / \sigma_c)^2$, where K_{Ic} is the fracture toughens and σ_c the tensile strength. Restricting his considerations to averaged approaches, Seweryn (1998) called these models nonlocal, being associated with assumption of the existence of a damage zone of finite length.

However even these approaches could fail in predicting the fatigue strength of a cracked or notched structure having sizes comparable to the critical distance. This occurs due to the assumption that it is just a material constant, thus not able to interact with the geometry under investigation. In this context, in order to overcome these incongruences, the coupled criterion of Finite Fracture Mechanics (FFM) was then introduced (Leguillon 2002, Cornetti et al. 2006). The model requires for crack propagation the simultaneous fulfilment of two conditions: a stress requirement and the energy balance. Accordingly, the distance becomes a structural parameter, depending both on l_{ch} and on the geometrical configuration. Thanks to its physically soundness and its efficiency, the criterion has been successfully applied to assess the strength of different materials, from polymers to ceramics, metals, rocks and composites, presenting different types of notch, and subjected to different loading conditions (see, for instance, Felger et al. 2017, 2019, Torabi et al. 2019, Sapora et al. 2020). It has been recently proved that FFM provides close predictions to the well-consolidated Cohesive Zone Model, once the constitutive law is properly defined (Cornetti and Sapora 2019; Cornetti et al. 2019: Doitrand et al. 2019).

In the present contribution, GE and FFM predictions will be compared by referring to the geometry depicted in Fig. 1, i.e. a borehole under internal pressure p, looking for a connection between the two internal lengths. The circular hole under isotropic biaxial tension has already been faced both through GE (Chen et al. 2018) and FFM (Sapora and Cornetti 2018), taking into account the previous works by Suknev (2015, 2020), Torabi et al. (2017), and Sapora et al. (2018) (see, also, Matvienko et al. 2019). In order to corroborate the related results, experimental data referring to rock materials taken from the Literature (Cuisat and Haimson 1992) are successfully implemented.

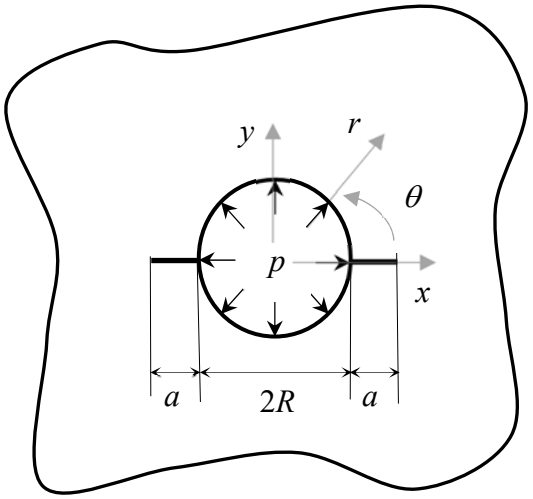

Fig. 1. Circular hole with radius *R* subjected to internal pressure *p*.

2. Introduction

A special form of gradient elasticity used in the present work, incorporates the Laplacian of the hydrostatic part of the strain tensor in Hooke's law. The complete analytical gradient solution for the displacement field of the problem requires extra boundary conditions on the second derivative of displacement. The value of the gradient coefficient *c* (equivalent to a square of the internal length) which is multiplied with the Laplacian of the hydrostatic part of the strain tensor is related with the characteristic scale of the material (for example the average grain size). The physical meaning of the gradient coefficient *c*, represents the distance over which a considerable variation of the elastic field takes place. In this section, a circular hole with radius *R*, under internal pressure *p* and remote biaxial (isotropic) tension σ, is investigated, as depicted in Fig. 1. A simple gradient constitutive model taking into account only the Laplacian of hydrostatic part of the strain tensor is used (Chen et al. 2018). The appropriate constitutive equation is

$$\sigma_{ij} = \lambda\varepsilon_{kk}\delta_{ij} + 2\mu\varepsilon_{ij} - c\lambda\nabla^2\varepsilon_{kk}\delta_{ij} \tag{1}$$

where λ,μ are Lame constants, δ_{ij} is the unit tensor (i.e., identity tensor components), ε_{ij} is the strain tensor, σ_{ij} is the stress tensor, ∇^2 is the Laplacian operator in polar coordinates, and *c* is the gradient coefficient. In polar coordinates, Eq. (1) reads in component form

$$\sigma_r = \left(\lambda+2\mu\right)\frac{\partial u}{\partial r} + \lambda\frac{u}{r} - c\lambda\frac{\partial^3 u}{\partial r^3} - 2c\lambda\frac{1}{r}\frac{\partial^2 u}{\partial r^2} + c\lambda\frac{1}{r^2}\frac{\partial u}{\partial r} - c\lambda\frac{u}{r^3} \tag{2a}$$

$$\sigma_\theta = \lambda\frac{\partial u}{\partial r} + \left(\lambda+2\mu\right)\frac{u}{r} - c\lambda\frac{\partial^3 u}{\partial r^3} - 2c\lambda\frac{1}{r}\frac{\partial^2 u}{\partial r^2} + c\lambda\frac{1}{r^2}\frac{\partial u}{\partial r} - c\lambda\frac{u}{r^3} \tag{2b}$$

For the axisymmetric plane strain configuration at hand, only the radial displacement exists ($u_r \neq 0$), whereas the tangential displacement vanishes ($u_\theta = 0$). Then, the expressions for the strain components become $\varepsilon_r = du_r / dr$ and $\varepsilon_\theta = u_r / r$. On neglecting the body forces, the only non-trivial equilibrium equation reads

$$\frac{d\sigma_r}{dr}+\frac{\sigma_r-\sigma_\theta}{r}=0 \tag{3}$$

Upon substitution of Eqs. (2a, b) into equilibrium Eq. (3), a fourth-order ordinary differential equation for u_r is obtained (Chen et al. 2018). Its general solution is easily derived as

$$u_r(r)=A\cdot r+\frac{B}{r}+C\cdot I_1\left(\frac{r}{\sqrt{c'}}\right)+D\cdot K_1\left(\frac{r}{\sqrt{c'}}\right) \tag{4}$$

where $c'=c\cdot\nu/(1-\nu)=l_g{}^2$, ν is the Poisson ratio, A,B,C,D are integration constants, whereas I_1 and K_1 are the first-order modified Bessel functions of first and second kind, respectively. In order to determine the integration constants in Eq. (6), four boundary conditions (two classical boundary conditions and two extra boundary conditions) are required: $\sigma_r\big|_{r=R}=-p$, $\sigma_r\big|_{r\to\infty}=0$, $d^2u/dr^2\big|_{r=R}=0$, and $d^2u/dr^2\big|_{r\to\infty}=0$. Then, the integration constants are calculated as follows:

$$A=0,\ B=\frac{pR^2}{2\mu}\left\{1+\frac{2c'K_1\left(\frac{R}{l_g}\right)}{RL_R}\right\},\ C=0,\ D=\frac{-pc'}{\mu L_R} \tag{5}$$

whereas $L_R=RK_1\left(\frac{R}{l_g}\right)+l_gK_0\left(\frac{R}{l_g}\right)$ and K_0 and K_1 are the zero and first-order modified Bessel functions of second kind. Inserting Eqs. (4) and (5) into Eq. (2b) yields:

$$\sigma_\theta=p\left[1+\frac{2l_g{}^2K_1\left(\frac{R}{l_g}\right)}{RL_R}\right]\frac{R^2}{r^2}-2p\left(\frac{l_g{}^2}{L_R}\right)\left[\frac{1}{r}K_1\left(\frac{r}{l_g}\right)+\frac{1}{l_g}K_0\left(\frac{r}{l_g}\right)\right] \tag{6}$$

At the boundary of the hole ($r=R$), the circumferential stress attains its maximum value

$$\sigma_\theta\big|_{r=R}=p-\frac{2p}{1+\left(\frac{R}{l_g}\right)\frac{K_1\left(\frac{R}{l_g}\right)}{K_0\left(\frac{R}{l_g}\right)}} \tag{7}$$

Equation (7) thus provides the stress concentration factor $\sigma_\theta(r=R)/p$, which will be used in Section 4 in order to calculate the dimensionless failure pressure.

3. Finite Fracture Mechanics

Let us consider the geometry represented in Fig. 1, where the reference system *xy* is centred at a circular hole with radius *R*. The coupled criterion of FFM (Carpinteri et al. 2009, Sapora et al. 2014) is based on the simultaneous fulfilment of two requirements.
The first is a stress condition:

$$\frac{1}{\overline{l}}\int_{1}^{1+\overline{l}} \sigma_y(\overline{x})d\overline{x} \geq \sigma_c \tag{8}$$

where $\overline{x} = x / R$, and $\overline{l} = l / R$ is the dimensionless crack advance. In simple terms, according to Eq. (8) the average circumferential stress σ_y in front of the hole edge must be greater than the tensile strength σ_c.

The second is the energy balance: the average energy release rate must be greater than the fracture energy. By means of Irwin's relationship, this condition can be expressed in terms of the stress intensity factor (SIF) K_I related to a small crack of length *a* stemming from the notch tip (Fig. 1), and its critical value K_{Ic}. Under mode I loading conditions, we have:

$$\sqrt{\frac{1}{\overline{l}}\int_{0}^{\overline{l}} K_I^2(\overline{a})\, d\overline{a}} \geq K_{Ic} \tag{9}$$

where $\overline{a} = a / R$ is the dimensionless crack length.
By referring to the case of a pressurized hole (Fig. 1), the stress field and SIF functions in Eqs. (8) and (9) can be expressed, respectively, as:

$$\sigma_y(\overline{x}) = \frac{p}{\overline{x}^2} \tag{10}$$

and

$$K_I(\overline{a}) = \sqrt{\pi R\overline{a}}\, pF_p(\overline{a}) \tag{11}$$

with

$$F_p(\overline{a}) = \frac{1}{1+\overline{a}}\left[0.637 + \frac{0.485}{\left(1+\overline{a}\right)^2} + 0.4\frac{\overline{a}^2}{\left(1+\overline{a}\right)^3}\right] \tag{12}$$

The shape function (12) was estimated to be accurate within 1% by Tada et al. (2000).
The substitution of Eq. (10) into Eq. (8) provides:

$$\frac{p}{\sigma_c} \geq 1 + \overline{l} \tag{13}$$

whereas inserting Eq. (11) into Eq. (9) yields:

$$\frac{p^2}{\sigma_c^2}\int_0^{\overline{l}} F_p^2(\overline{a})\overline{a}d\overline{a} \geq \frac{\overline{l}}{\pi}\frac{l_{ch}}{R} \tag{14}$$

The parameter $l_{ch} = (K_{Ic} / \sigma_c)^2$, also known as Irwin's length, is an indicator of the brittleness of the material: the more brittle the material (low toughness and high strength), the smaller l_{ch}.

4. Discussion of results

GE and FFM models developed in the previous section will be now compared. As stated before, both models are based on an internal length, l_g for GE and l_{ch} for FFM. In order to compare the related results, let us now introduce a proportionality coefficient β so that:

$$l_g = \beta\, l_{ch} \tag{15}$$

In case of a pressurized hole, according to Eq. (7), the dimensionless critical pressure for GE reduces to:

$$\frac{p_f}{\sigma_c} = \frac{1}{1-\dfrac{2}{1+\dfrac{R}{l_g}\dfrac{K_1\left(R/l_g\right)}{K_0\left(R/l_g\right)}}} \tag{16}$$

Note that the geometry is locally positive and globally negative, since the SIF (11) is first increasing (starting from zero) and then tending again to zero as R tends to infinite. According to FFM, we find that two scenarios are possible. For radii R larger than $R^* \approx 0.4\ l_{ch}$, the crack propagation is first unstable (however turning stable after a certain growth): the crack onset takes place when both inequalities (8) and (9) are strictly fulfilled:

$$\begin{cases} (1+\overline{l}_c)^2\displaystyle\int_0^{\overline{l}_c} F_p^2(\overline{a})\overline{a}d\overline{a} = \frac{l_{ch}}{\pi R} \\ \dfrac{p_f}{\sigma_c} = 1+\overline{l}_c \end{cases} \tag{17}$$

On the other hand, for radii R below R^*, the crack propagation is stable from the beginning and the onset is provided by the minimum of the discrete energy balance.
In formulae, from Eq. (14):

$$\frac{p_f}{\sigma_c} = \sqrt{\frac{l_{ch}}{\pi R}\frac{1.29}{\displaystyle\int_0^{1.29} F_p^2(\overline{a})\overline{a}d\overline{a}}} = \sqrt{2.10\frac{l_{ch}}{R}} \tag{18}$$

$\overline{l}^* \approx 1.29$ being the point where the SIF intersects its average function (coinciding with the point where the average SIF function attains its maximum value (Weißgraeber et al. 2016)). In this case, the stress requirement (13) is trivially (over) fulfilled. Of course, the crack propagation reveals to be stable ($dK_I / da < 0$), and the infinitesimal crack onset at the subsequent steps will be described by LEFM (K_I=K_{IC}): subsequent increases in pressure are required to cause continued crack propagation.

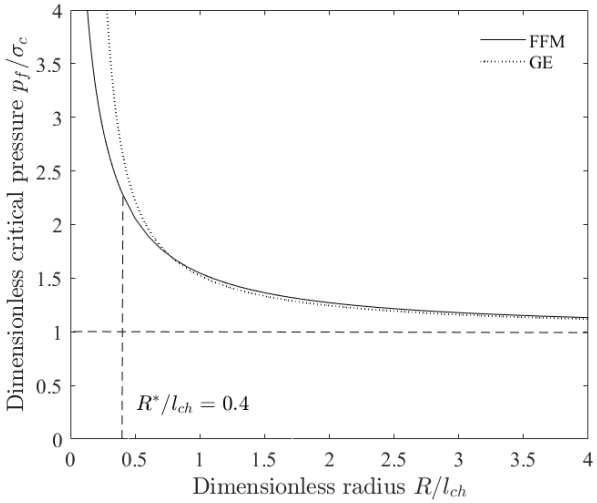

Fig. 2. Pressurized hole: critical pressure via FFM and GE by setting $\beta = 0.24$ in Eq. (15).

FFM and GE predictions (by setting again $\beta = 0.24$ in Eq. (15)) are reported in Fig. 2: the matching is excellent except for vanishing radii, where indeed both criteria predict a divergent critical pressure. The asymptotic limit $p_f \rightarrow \sigma_c$ is approached for increasing radii. It should be noted that the range where GE and FFM nearly coincide are generally those of practical interest, as it will be clear in the next section.

4.1 Comparison with experimental data

In order to verify the accuracy of the proposed relationship, we need a comparison with experimental data. Cuisat and Hamison (1992) investigated the effect of size on hydraulic fracturing breakdown pressure under zero far-field stresses by testing Lac du Bonnet granite. The material strength σ_c was measured experimentally, resulting in 8.1 MPa. The fracture toughness K_{Ic} was assumed equal to 0.35 MPa $\sqrt{\text{m}}$, thus providing $l_{ch} \approx 1.87$ mm on the basis of point method arguments (Louks et al. 2014). FFM results are plotted in Fig. 3, together with GE results implementing $l_g \approx 0.449$ mm via Eq. (15). As it can be seen, the agreement is more than satisfactory for both approaches.

5. Conclusions

Gradient Elasticity and Finite Fracture Mechanics were applied to the borehole problem. The two models are generated by completely different approaches: GE is based on a nonlocal stress-strain relationship, and it considers the (size-dependent) stress concentration factor, i.e. the inverse quantity of normalized critical pressure, as the governing failure parameter; FFM is based on a classical local constitutive law, and it considers the fulfilment of two stress and energy (average) conditions for fracture propagation. In this optic, once the stress field is known, GE can be even more straightforward for applications, since it requires the implementation of just one single equation. Both models are based on a characteristic (internal) length: l_g for GE and l_{ch} for FFM, both connected to the microstructure of the material. By considering the following proportionality law, $l_g = 0.24\ l_{ch}$, it has been shown that GE and FFM predictions are in excellent agreement over the range of practical engineering interest, matching the experimental data available in the Literature. This a key point, since l_g can be linked straightforwardly to the brittleness of the material for future GE applications.

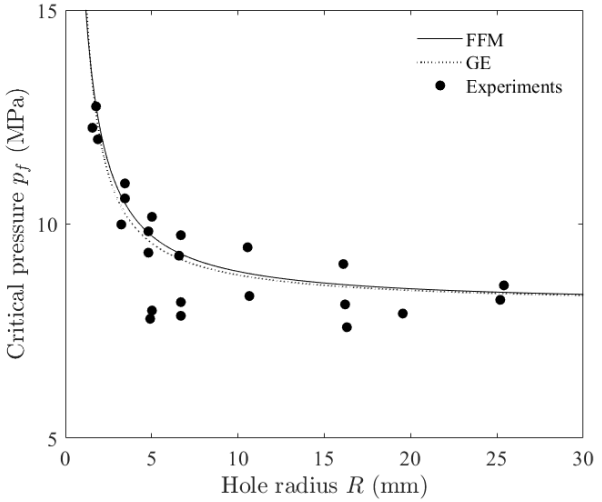

Fig. 3. Pressurized hole: FFM and GE predictions vs. experimental data (granite, Cuisat and Haimson (1992)).

References

Aifantis, E.C. 1984. On the microstructural origin of certain inelastic models. J. Mat. Engng. Tech. 106, 326–330

Aifantis, E.C. 1987. The physics of plastic deformation. Int. J. Plasticity 3, 211–247.

Aifantis, E.C. 1992. On the role of gradients in the localization of deformation and fracture. Int. J. Eng. Sci. 30, 1279–1299.

Askes, H., Aifantis, E.C. 2011. Gradient elasticity in statics and dynamics: an overview of formulations, length scale identification procedures, finite element implementations and new results, Int. J. Solids Struct. 48, 1962–1990.

Carpinteri, A., Cornetti, P., Pugno, N., Sapora, A., Taylor, D. 2009. Generalized fracture toughness for specimens with re-entrant re-entrant corners: experiments vs. theoretical predictions. Struct. Eng. Mech. 32, 609–620.

Cornetti, P., Sapora, A. 2019. Penny-shaped cracks by finite fracture mechanics. Int. J. Fract. 219, 153–159.

Cornetti, P., Pugno, N., Carpinteri, A., Taylor, D. 2006. Finite fracture mechanics: a coupled stress and energy failure criterion. Eng. Fract. Mech. 73, 2021–33.

Cornetti, P., Muñoz-Reja, M., Sapora, A., Carpinteri, A. 2019. Finite fracture mechanics and cohesive crack model: Weight functionsvs. cohesive laws. Int J Solids Struct 156–157, 126–136.

Chen, H., Qi, C., Efremidis, G., Dorogov, M., Aifantis, E.C. 2018. Gradient elasticity and size effect for the borehole problem. Acta Mech 229, 3305–3318.

Cuisat, F.D., Haimson, B.C. 1992. Scale effects in rock mass stress measurements. International Journal of Rock Mechanics and Mining Sciences & Geomechanics Abstracts 29, 99-117.

Doitrand, A., Estevez, R., Leguillon, D. 2019. Comparison between cohesive zone and coupled criterion modeling of crack initiation in rhombus hole specimens under quasi-static compression. Theor. Appl. Fract. Mech. 99, 51–59.

Efremidis, G., Carpinteri, A., Aifantis, E.C. 2001. Griffith theory versus gradient elasticity in the evaluation of porous materials tensile strength. J Mech Behav Mats 12, 95-105

Eringen, A.C. 1983. On differential equations of nonlocal elasticity and solutions of screw dislocation and surface waves. J. Appl. Phys. 54, 4703-4710.

Eringen, A.C., Speziale, C.G., Kim, B.S. 1972. Crack tip problems in nonlocal elasticity. J. Mech. Phys. Solids 25, 339-355.

Felger, J., Stein, N., Becker, W. 2017. Mixed-mode fracture in open-hole composite plates of finite-width: An asymptotic coupled stress and energy approach. Int. J. Solid. Struct. 122–123, 14–24.

Felger, J.; Rosendahl, P.L.; Leguillon, D.; Becker, W. 2019. Predicting crack patterns at bi-material junctions: A coupled stress and energy approach. Int. J. Solids Struct.164, 191–201.

Kunin, I.A. 1983. Theory of Elastic Media with Microstructure, Springer-Verlag, Berlin.

Leguillon, D. 2002. Strength or toughness? A criterion for crack onset at a notch. Eur J Mech A/Solids 21, 61–72.

Louks, R., Askes, H., Susmel, L. 2014. Static assessment of brittle/ductile notched materials: an engineering approach based on the Theory of Critical Distances, Frattura ed Integrità Strutturale 8, 23–30.

Matvienko, Yu. G., Pisarev, V.S., Eleonsky, S.I. 2019. The effect of low-cycle fatigue on evolution of fracture mechanics parameters in

residual stress field caused by cold hole expansion. Frattura ed Integrità Strutturale 47, 303-320.
Mindlin, R.D. 1965. Second gradient of strain and surface tension in linear elasticity. Int. J. Solids Struct. 1, 417-438.
Sapora, A., Cornetti, P. 2018. Crack onset and propagation stability from a circular hole under biaxial loading. Int J Fract 214, 97-104.
Sapora, A., Cornetti, P., Carpinteri, A. 2014. V-notched elements under mode II loading conditions. Struct Eng Mech 49, 499–508.
Sapora, A., Torabi, A.R., Etesam, S., Cornetti, P. 2018. Finite Fracture Mechanics crack initiation from a circular hole. Fatigue Fract. Eng. Mater. Struct 4.1, 1627–1636.
Sapora, A., Cornetti, P., Campagnolo, A., Meneghetti, G. 2020. Fatigue limit: Crack and notch sensitivity by Finite Fracture Mechanics. Theor. Appl. Fract. Mech. 105,102407.
Seweryn, A. 1998. A non-local stress and strain energy release rate mixed mode fracture initiation and propagation criteria. Eng. Fract. Mech. 59:737–760.
Suknev, S.V. 2015. Fracture of brittle geomaterial with a circular hole under biaxial loading. J. Appl. Mech. Tech. Phy. 56:1078–1108.
Suknev, S.V. 2020. Brittle and Quasi-Brittle Fracture of Geomaterials with Circular Hole in Nonuniform Compression. Journal of Mining Science 56, 174–183.
Tada, H., Paris, P., Irwin, G. 2000. The stress analysis of cracks handbook, 3rd edn. Paris Productions Incorporated, StLouis.
Taylor, D. 2007. The Theory of Critical Distances. A New Perspective in Fracture Mechanics, Elsevier, London.
Torabi, A.R., Etesam, S., Sapora, A., Cornetti, P. 2017. Size effects on brittle fracture of Brazilian disk samples containing a circular hole. Eng. Fract. Mech. 186, 496–503.
Torabi, A.R., Berto, F., Sapora, A. 2019. Finite Fracture Mechanics Assessment in Moderate and Large Scale Yielding Regimes. Metals 9:602.
Weißgraeber, P., Hell, S., Becker, W. 2016. Crack nucleation in negative geometries. Eng. Fract. Mech. 168, 93–104.